Tracking electron motion within and outside of Floquet bands from attosecond pulse trains in time-resolved ARPES

OPEN ACCESS
IOP Publishing
Journal of Physics: Condensed Matter
J. Phys.: Condens. Matter **36** (2024) 225401 (13pp)
https://doi.org/10.1088/1361-648X/ad2a0e

Tracking electron motion within and outside of Floquet bands from attosecond pulse trains in time-resolved ARPES

Ofer Neufeld[1,*], **Hannes Hübener**[1], **Umberto De Giovannini**[1,2] **and Angel Rubio**[1,3,*]

[1] Max Planck Institute for the Structure and Dynamics of Matter and Center for Free-electron Laser Science, Hamburg 22761, Germany
[2] Università degli Studi di Palermo, Dipartimento di Fisica e Chimica—Emilio Segrè, Palermo I-90123, Italy
[3] Center for Computational Quantum Physics (CCQ), The Flatiron Institute, New York, NY 10010, United States of America

E-mail: oneufeld@schmidtsciencefellows.org and angel.rubio@mpsd.mpg.de

Received 12 December 2023, revised 6 February 2024
Accepted for publication 16 February 2024
Published 7 March 2024

Abstract

Floquet engineering has recently emerged as a technique for controlling material properties with light. Floquet phases can be probed with time- and angle-resolved photoelectron spectroscopy (Tr-ARPES), providing direct access to the laser-dressed electronic bands. Applications of Tr-ARPES to date focused on observing the Floquet-Bloch bands themselves, and their build-up and dephasing on sub-laser-cycle timescales. However, momentum and energy resolved sub-laser-cycle dynamics between Floquet bands have not been analyzed. Given that Floquet theory strictly applies in time-periodic conditions, the notion of resolving sub-laser-cycle dynamics between Floquet states seems contradictory—it requires probe pulse durations below a laser cycle that inherently cannot discern the time-periodic nature of the light-matter system. Here we propose to employ attosecond pulse train probes with the same temporal periodicity as the Floquet-dressing pump pulse, allowing both attosecond sub-laser-cycle resolution and a proper projection of Tr-ARPES spectra on the Floquet–Bloch bands. We formulate and employ this approach in *ab-initio* calculations in light-driven graphene. Our calculations predict significant sub-laser-cycle dynamics occurring within the Floquet phase with the majority of electrons moving within and in-between Floquet bands, and a small portion residing and moving outside of them in what we denote as 'non-Floquet' bands. We establish that non-Floquet bands arise from the pump laser envelope that induces non-adiabatic electronic excitations during the pulse turn-on and turn-off. By performing calculations in systems with

* Authors to whom any correspondence should be addressed.

poly-chromatic pumps we also show that Floquet states are not formed on a sub-laser-cycle level. This work indicates that the Floquet-Bloch states are generally not a complete basis set for sub-laser-cycle dynamics in steady-state phases of matter.

Supplementary material for this article is available online

Keywords: ARPES, floquet, TDDFT, nonlinear optics, ultrafast spectroscopy, attosecond science

1. Introduction

Tailoring material electronic structure and optoelectronic properties with laser irradiation has gained considerable attention in the condensed matter and materials community over the last decade [1–21]. Within this approach, a solid system is driven by light into an out-of-equilibrium steady-state phase (Floquet phase) that exhibits time-periodic behavior [22], and potentially displays different properties from the non-driven ground state [18]. Such methodology has for instance enabled turning insulators into conductors and vice versa [11], tuning material topology [23–30], and arbitrarily controlling the shape of the electronic band structure [5]. This represents an exciting alternative avenue to the standard approach of either searching for new material systems with desired properties [31, 32], or synthetically tailoring properties by introducing doping, defects, pressure, temperature, etc.

In order to fully capitalize on these capabilities, it is essential to understand the fundamental electron dynamics that supports the steady-state out-of-equilibrium phase. Inevitably, such dynamics are responsible for emerging observables such as transport phenomena [33–35] or high harmonic generation (HHG) [36, 37]. The most direct methodology that allows exploring Floquet phases of matter is time- and angle-resolved photoelectron spectroscopy (Tr-ARPES), whereby a short probe pulse ionizes the sample while it is irradiated by a dressing pump laser pulse (which can also be applied in a spin-resolved manner). The resulting momentum-resolved photoelectron spectra image the population of electronic bands within the material, resolved on the time-scale of the probe pulse duration. This technique was successfully used to observe Floquet-Bloch bands and sidebands [2, 38], Floquet-related gap opening and band hybridization [39], charge dynamics in topological surface states and their coupling to the continuum [40–42], photoionization time delays [43–45], and more [46]. Very recently, it was also employed for uncovering the coherent build-up and subsequent dephasing of the Floquet phase itself with sub-laser-cycle resolution [47, 48]. However, no work to date has analyzed the energy and momentum resolved sub-laser-cycle motion of charges between the Floquet–Bloch states in ARPES. To clarify, an observation of this type of charge motion is of inherently contradictory nature: the Floquet states are only properly defined in time-periodic conditions (as eigenstates of a time-averaged effective Hamiltonian), resulting in time-fixed occupation indices [22]. Indeed, this is the property that makes the Floquet–Bloch states so appealing for analyzing physical effects and for tuning material properties. To measure time-changing occupations of Bloch states would imply that the dynamics are not time-periodic, and cannot be described within Floquet theory. Put differently, a probe pulse would need to have a sub-laser-cycle duration to observe such dynamics, meaning that it cannot 'sense' the time-periodic nature of the system. In such conditions instantaneous Houston states are often considered the more appropriate basis for describing electron dynamics [49–51], and within the Floquet basis the dynamics are described as micromotion or non-stroboscopic dynamics [52–56]. While it is possible to transform between the two basis sets, it would be much more appealing to have a technique that directly allows to project the ARPES spectra onto the Floquet–Bloch states instead, while keeping the attosecond temporal resolution. This would allow to distinguish and immediately observe any emerging out-of-equilibrium phenomena in real-time, a property which the instantaneous Huston states do not permit given their adiabatically evolving nature.

Here we propose a methodology for overcoming these limitations and implement it numerically. We use attosecond pulse train probes that exhibit the same temporal periodicity as the pump Floquet-dressing pulses [57, 58]. Thus, the probe pulse samples the light-driven material once-per-cycle, over multiple laser cycles, meaning that the Floquet-Bloch states should be a good basis set for the dynamics. At the same time, attosecond resolution is maintained and charge dynamics can be directly resolved by tuning the pump-probe delay. This allows deciphering sub-laser-cycle charge dynamics without performing additional projections or transformations. We employ this technique within *ab-initio* time-dependent density functional theory (TDDFT) [59], and use it to analyze dynamics in laser-driven graphene. Our results predict the existence of significant attosecond charge motion between Floquet–Bloch bands during the course of a laser cycle. Moreover, charge dynamics also occurs outside of the Floquet–Bloch bands in what we denote as 'non-Floquet' bands, suggesting that they do not form a complete basis set for sub-laser-cycle dynamics. We analyze the physical origin of non-Floquet bands and show that their formation is associated with breaking of time-periodicity in the pump laser pulse temporal envelope. We further employ the technique in poly-chromatically-driven graphene in conditions where each laser half-cycle is approximately circularly-polarized with an alternating handedness. Our analysis resolves the ARPES contributions from separate half-cycles, showing that a Floquet gap does not open in each half cycle even though time-reversal symmetry (TRS) is broken locally in time, contrary to intuitive expectations. This result implies that a longer duration

build-up of Floquet dynamics is perquisite for controlling material band structure with light.

The paper is organized as follows: section 2 formulates the methodology of the technique and its implementation within TDDFT. Section 3 presents results from quasi-monochromatically- and poly-chromatically-driven graphene, analyzing attosecond charge dynamics within and outside of the Floquet-Bloch bands. Finally, section 4 summarizes our results and presents a future outlook.

2. Methodology

2.1. Laser-driven dynamics

We begin by outlining our methodological first-principles approach. All calculations were performed using the open-access real-space grid-based code, Octopus [60–63]. Within this approach, the electron dynamics in the light-driven material are described fully quantum mechanically and *ab-initio* in the framework of real-time TDDFT [59]. We employed the adiabatic and local density approximation for the exchange correlation (XC) functional, and assumed clamped nuclei. We also ignored the spin degree of freedom and spin-orbit interactions as those are negligible in graphene. The laser-matter interaction was described in the velocity gauge and dipole approximation. The resulting equations of motion for the Kohn-Sham-Bloch (KSB) states are given in atomic units by:

$$i\partial_t \left|\varphi^{KS}_{n,\mathbf{k}}(t)\right\rangle = \left(\frac{1}{2}\left(-i\nabla + \frac{\mathbf{A}(t)}{c}\right)^2 + v_{KS}(\mathbf{r},t)\right)\left|\varphi^{KS}_{n,\mathbf{k}}(t)\right\rangle \tag{1}$$

where $\left|\varphi^{KS}_{n,\mathbf{k}}(t)\right\rangle$ is the KSB state at k-point $\mathbf{k}$ and band index n, $\mathbf{A}(t)$ is the total vector potential of all laser pulses interacting with the material such that $-\partial_t \mathbf{A}(t) = c\mathbf{E}(t)$, with c the speed of light. $v_{KS}(\mathbf{r},t)$ is the time-dependent KS potential given by:

$$v_{KS}(\mathbf{r},t) = V_{ion} + \int d^3r' \frac{n(\mathbf{r}',t)}{|\mathbf{r}-\mathbf{r}'|} + v_{XC}[n(\mathbf{r},t)] \tag{2}$$

where V_{ion} describes the sum of all electrostatic interactions between electrons and nuclei, including interactions with core electrons that are handled by a frozen-core approximation with appropriate pseudopotentials [64]. v_{XC} is the XC potential that is a functional of $n(\mathbf{r},t) = \sum_{n,k}\left|\left\langle \mathbf{r}|\varphi^{KS}_{n,k}(t)\right\rangle\right|^2$, the time-dependent electron density. Equations (1) and (2) are propagated in real-time (with a temporal spacing of $\Delta t = 3.6$ attoseconds) on a real-space grid (with spacing $\Delta x = 0.38$ Bohr). The initial states at $t = 0$ are taken as the KS ground state that is found within DFT on a similar level of theory using the experimental lattice configuration (perfect honeycomb structure with a lattice parameter of $a_0 = 2.456$ Å), and with an employed Γ-centered k-space grid of $12 \times 12 \times 1$ k-points, where the xy plane hosts the graphene sheet (employing periodic boundaries for one primitive unit cell), and the z-axis is taken as a non-periodic axis with additional vacuum spacing of 55 Bohr in each direction. During propagation we added a complex absorbing potential with a $\sin^2(z)$ shape [65] of width 30 Bohr and amplitude 1 Hartree on both sides of the graphene monolayer to avoid spurious reflection of electrons at the boundaries.

We further included an artificial doping of the graphene conduction band (CB) to make ARPES contributions from higher lying bands visible in the spectra. This was achieved following [66], by adding additional 0.35 $\bar{e}$ charge per unit cell, which was compensated by an attractive potential arising from the classical charge density:

$$\rho_{\text{dope}}(\mathbf{r}) = N\exp\left\{-5z^2\right\} \tag{3}$$

where $N = 0.02359$ is a normalization constant that assures charge from ρ_{dope} integrates to -0.35 $\bar{e}$ per unit cell and the system is neutral. Practically, ρ_{dope} electrostatically binds the additional doping charges on the graphene monolayer, which is roughly analogous to the experimental techniques of a gate potential-induced doping, and only slightly perturbs the electronic bands. Notably, the results presented below do not depend on the doping procedure itself, which is only used for visualizing high-lying bands more easily.

The KSB equations of motion were also solved on an auxiliary k-grid that did not contribute to the total charge density ($n(\mathbf{r},t)$), but upon which the ARPES calculations detailed below took place. We used two grids passing directly through the K point, parallel to k_x or k_y (with 144 k-points and a length of a third of a reciprocal lattice vector).

All calculations presented in the main text employed the independent particle approximation (IPA), in which the dynamical evolution of the KS potential was frozen: $v_{KS}(\mathbf{r},t) \cong v_{KS}(\mathbf{r},t=0)$. We have found this to be a very good approximation for the driven electron dynamics in our conditions. All numerical parameters were tested for convergence.

2.2. Tr-ARPES calculations

ARPES spectra were obtained by a 'numerical experiment' methodology, whereby we aimed to simulate the measurement process as it occurs in the lab. The laser vector potential in equation (1) included two terms:

$$\mathbf{A}(t) = \mathbf{A}_{\text{pump}}(t) + \mathbf{A}_{\text{probe}}(t). \tag{4}$$

Here $\mathbf{A}_{\text{pump}}(t)$ refers to the pump field that dresses the system and causes it to enter a so-called Floquet steady-state phase. For the quasi-monochromatic laser pumped cases, this field was taken to have the form:

$$\mathbf{A}_{\text{pump}}(t) = f(t)\frac{cE_0}{\omega}\sin(\omega t)\hat{\mathbf{e}} \tag{5}$$

where $f(t)$ is the following temporal envelope function that was taken to have a 'super-sine' form [67]:

$$f(t) = \left(sin\left(\pi\frac{t}{T_p}\right)\right)^{\left(\frac{\left|\pi\left(\frac{t}{T_p}-\frac{1}{2}\right)\right|}{\sigma}\right)} \tag{6}$$

with $\sigma = 0.75$ ($f(t)$ resembles a super-Gaussian but is more numerically convenient) and a total pulse duration of 16 laser cycles $T_p = 16T$ (with a full-width-half-max of 8 laser cycles), where ω is the carrier wave associated with the fundamental period, $T = \frac{\omega}{2\pi}$. For some calculations in section 3.2 we vary the envelope shape by choosing different values for σ. Note that results obtained in this paper do not depend on the particular shape of the temporal envelope function and we used this form for convenience. E_0 in equation (5) is the field amplitude, ω is the carrier frequency, and $\hat{\mathbf{e}}$ is a unit vector taken either linearly-polarized transverse to the carbon-carbon bonds (along the x-axis), or circularly polarized.

For the poly-chromatic laser-driven cases we employed a tri-chromatic pump laser field of the form:

$$\mathbf{A}_{\text{pump}}(t) = f(t)\frac{cE_0}{\omega}\left(\sin(\omega t)\hat{\mathbf{x}} + \sin(2\omega t)\hat{\mathbf{y}} - \sin(3\omega t)\hat{\mathbf{x}}\right). \tag{7}$$

The Lissajous curve traced-out by this time-dependent electric field is visualized in figure 7—it roughly resembles a circularly-polarized laser field of frequency 2ω, but where the field helicity flips its handedness every half-cycle. Thus, the overall pump field in equation (7) respects TRS [68], but still breaks it locally-in-time when considering its individual half-cycles as separate pumping entities. Notably, since the field in equation (7) involves carrier frequencies that are integer multiples of the fundamental frequency, ω, it still respects T-periodicity, permitting the application of Floquet theory.

The probe pulse, $\mathbf{A}_{\text{probe}}(t)$, is taken as linearly-polarized along the z-axis (transverse to the graphene monolayer), with an extreme ultraviolet (XUV) carrier frequency of $\omega_{\text{xuv}} = 80$ eV:

$$\mathbf{A}_{\text{probe}}(t) = f_{\text{xuv}}(t)\frac{cE_{\text{xuv}}}{\omega_{\text{xuv}}}\sin(\omega_{\text{xuv}}t) f_{\text{train}}(t - t_0)\hat{\mathbf{z}} \tag{8}$$

where $f_{\text{xuv}}(t)$ is an envelope function taken similar to that in equation (6), but such that its FWHM is roughly similar to that of the corresponding pump pulse (and where in section 3.2 we vary the envelope parameter σ for studying effects of the probe pulse duration). f_{train} denotes a time-periodic gating function that has the same periodicity as the pump field, and t_0 is an intra-cycle pump-probe delay (an inter-cycle pump-probe delay is not considered here as it is irrelevant for tracking sub-cycle dynamics). For the standard ARPES conditions with a long-duration XUV probe, we simply choose $f_{\text{train}} = 1$. As we will show, this corresponds to the case of obtaining ARPES spectra that follows the expected Floquet quasi-energy band structure, since the probe continuously samples the steady-state phase of the driven system (see illustration in figure 1(a)). For choosing an attosecond pulse train probe, we set the train function to one of two forms: (i) a highly temporally-resolved form:

$$f_{\text{train}}(t) = \cos^{40}\left(\frac{\omega}{2}t\right), \tag{9}$$

which provides an intra-cycle FWHM of 0.084 T (see illustration in figure 1(b)). (ii) A half-cycle temporally-resolved form where the probe train covers half of the temporal range of one pump laser cycle:

$$f_{\text{train}}(t) = 0.5\left(1 + \tanh\left(5\cos(\omega t)\right)\right), \tag{10}$$

providing an intra-cycle FWHM of 0.52 T (see illustration in figure 1(c)). E_{xuv} is the probe's peak amplitude, taken in the linear-response regime to correspond to an intensity of 2×10^8 W cm^{-2}.

Overall, the pump laser field dresses the solid, causing it to enter into a Floquet steady-state phase of matter. The probe pulses (either temporally resolved or not) photo-ionize electrons that are recorded in a momentum-resolved manner as the emerging ARPES spectra. The pump-probe delay can be scanned to provide Tr-ARPES spectra with a temporal resolution of the probe pulse duration (or intra-cycle duration in the case of attosecond pulse trains).

The ARPES spectra are calculated from the time-dependent KSB states on the auxiliary k-grid using the surface-flux method T-SURFF [69, 70]. Within this approach the momentum-resolved flux of photoelectrons is recorded across a surface (**S**) normal to the graphene monolayer, which lies sufficiently far away in the continuum to avoid interactions of outgoing waves with the monolayer (25 Bohr away from the monolayer plane, in region $z >$ **S** Bohr). This surface is also sufficiently far from the monolayer in order to approximate outgoing waves as a superposition of Bloch-Volkov states, $|\chi_{\mathbf{p}}(t)\rangle$, where further interaction with other electrons is neglected. $\mathbf{p}$ denotes the state momenta that is represented on a finite Fourier grid. The states in this region interact purely with the Volkov Hamiltonian, $H_V(t) = \frac{1}{2}\left(-i\nabla + \frac{\mathbf{A}(t)}{c}\right)^2$, and their dynamics can be solved analytically. Since Bloch-Volkov states form a complete basis set in the region beyond **S**, we can formally decompose the KSB states into a sum of Volkov states, $\left|\varphi^{KS}_{n,\mathbf{k}}(t)\right\rangle = \int \mathrm{d}\mathbf{p} b_{n,\mathbf{k}}(\mathbf{p},t)\left|\chi_{\mathbf{p}}(t)\right\rangle$, with the coefficients $b_{n,\mathbf{k}}(\mathbf{p},t)$ calculated according to a flux integral (with the $\mathbf{k}$ index referring to a point along the auxiliary k-grid upon which ARPES is calculated):

$$b_{n,\mathbf{k}}(\mathbf{p},t) = -\int_0^t \mathrm{d}\tau \oint_S \mathrm{d}\mathbf{s}\langle\chi_{\mathbf{p}}(\tau)\left|\hat{j}(\tau)\right|\varphi^{KS}_{n,\mathbf{k}}(\tau)\rangle \tag{11}$$

with $\hat{j}(t)$ the single-particle current density operator, $\hat{j}(t) = \frac{1}{2}\left(-i\nabla + \frac{\mathbf{A}(t)}{c} + \text{c.c.}\right)$. Equation (11) can be further simplified by substituting the KSB state with its spatially-periodic part and k-dependent phase. From equation (11) the momentum (and energy) resolved photoelectron spectra is obtained by summing over all occupied bands and evaluating the flux and the end of the simulation: $I_{\mathbf{k}}(\mathbf{p}) = \sum_n |b_{n,\mathbf{k}}(\mathbf{p}, t \to \infty)|^2$.

2.3. Removing continuum effects

As discussed above, the T-SURFF methodology divides the simulation box into: (i) an inner region up to the electron

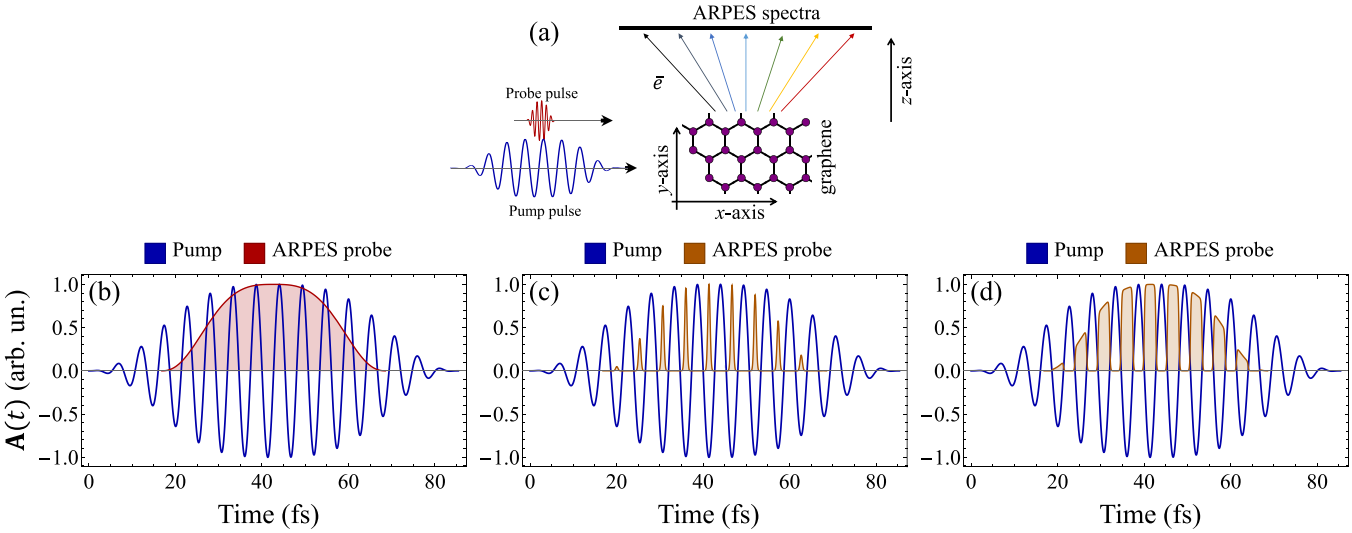

Figure 1. (a) Illustration of Tr-ARPES pump-probe set-up used here. A monolayer of graphene is irradiated by an intense pump pulse that is polarized in the monolayer plane (blue, *xy* plane), which dresses the electronic system and causes it to enter a steady-state Floquet phase. A weak XUV probe pulse polarized transverse to the monolayer (along the *z*-axis) photoionizes electrons which propagate up to the detector surface, at which point their momenta and energy is recorded. (b) Illustration of standard Tr-ARPES conditions for observing Floquet phases of matter—the ARPES probe pulse (red) has a temporal duration comparable to multiple pump laser cycles, thus sensing the time-periodic nature of the electronic dynamics (with $f_{\text{train}}(\text{t}) = 1$). (c) Illustration of Tr-ARPES with an attosecond train probe pulse that has the same periodicity as the pump pulse in highly temporally-resolved conditions (with $f_{\text{train}}(\text{t})$ as in equation (9)). (d) Same as (c) but for conditions where the intra-cycle temporal resolution of the attosecond train is half of a pump cycle ($f_{\text{train}}(\text{t})$ as in equation (10)).

flux recording surface, in which electrons are treated with TDDFT; and (ii), an outer region where electrons are treated as Volkov states. Consequently, during their propagation in the outer region the electron momenta continue to be modulated by interactions with the laser (this effect it commonly known as 'streaking'). However, in order to temporally resolve ARPES spectra with sub-cycle resolution, this effect must be suppressed—if it is not, then electronic wavepackets propagating in the continuum will interact with multiple laser cycles up to the detector, spoiling the temporal resolution (as we wish to resolve contributions to ARPES spectra coming from only specific moments in time within the laser cycle). Moreover, spectra containing contribution of continuum states to the dynamics inherently also includes physical effects that occur outside of the material system, and have nothing to do with laser-dressed phases of matter. To numerically avoid such effects here, we artificially employed a spatial envelope on the pumping laser field in equation (4): $\mathbf{A}_{\text{pump}}(t) \to \mathbf{A}_{\text{pump}}(t,z) = \Theta(z)\,\mathbf{A}_{\text{pump}}(t)$, where $\Theta(z)$ is the following spatial envelope:

$$\Theta(z) = M\left\{\text{erf}\left(\frac{z+z_0}{w}\right) - \text{erf}\left(\frac{z-z_0}{w}\right)\right\} \qquad (12)$$

where $M = 0.5/\text{erf}(z_0/w)$ is a normalization constant, $z_0 = 7$ Bohr is the spatial extent of the envelope above and below the graphene monolayer (chosen as the position where the electronic wave functions have spatially decayed), and $w = 0.5$ Bohr is the width of the vector potential decay region. The envelope in equation (12) guarantees that electrons only 'feel' an electric field in the spatial region of the graphene monolayer. Thus, this approach overall assures that emerging ARPES spectra only contain information about the Floquet phase of matter within the material, with the spectra temporally resolved on the timescale of the probe. Practically, this means the vector potential is assumed zero outside **S** and the Volkov states reduce to free electron states. We further note that from a physical perspective applying $\Theta(z)$ means relinquishing the dipole approximation, which should also generate a magnetic field. However, here we completely ignore such phenomena and use $\Theta(z)$ as a numerical 'shortcut' for fully removing continuum contributions in ARPES.

3. Attosecond electron dynamics

3.1. Quasi-monochromatic pump fields

We now explore Tr-ARPES in graphene using the setup and methodology described above. We begin with a quasi-monochromatic circularly-polarized pump pulse (CPL). In these conditions it is well established that the linearly-dispersing Dirac bands in graphene split, lifting the degeneracy at K, causing a quasi-energy gap opening throughout the Brillouin zone (BZ). Moreover, due to the breaking of TRS by the CPL the resulting Floquet bands are of topological nature and support topologically protected Floquet surface states [18].

The *ab-initio* calculations presented in figure 2(a) show the expected physical behavior, validating our methodology—a large energy gap of ∼0.5 eV opens up at K in our chosen driving regime. The ARPES spectra in figure 1(a) is overlayed with the calculated quasi-energy Floquet bands for the CPL pump case (dashed white), which were calculated with a 5th-order tight-binding model in an approach fully described in [66]. The

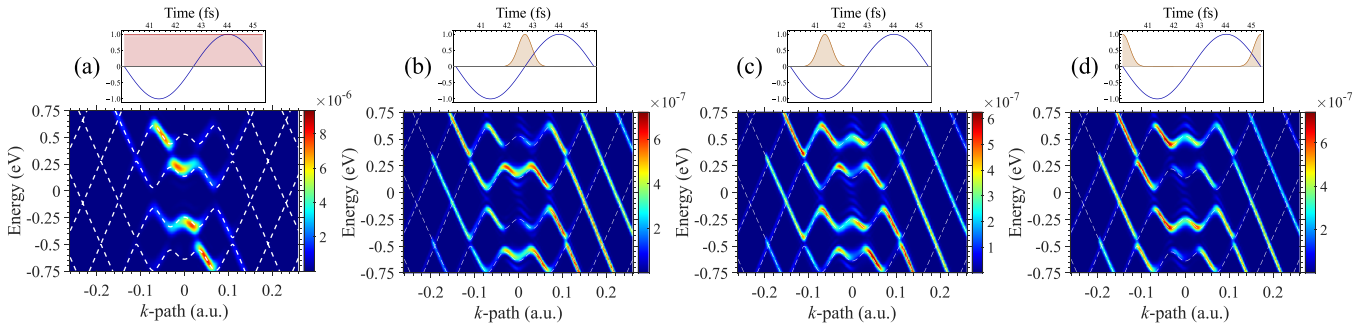

Figure 2. Tr-ARPES spectra with a quasi-monochromatic circularly-polarized pump field (1600 nm, $I_0 = 10^{11}$ W cm^{-2}) probed parallel to k_y. (a) ARPES spectra in the standard conditions where sub-cycle contributions to spectra are not resolved. The spectra are shifted such that the zero points indicates K. (b)–(d) Tr-ARPES spectra probed by attosecond train (with f_{train}(t) as in equation (9)) for different pump-probe delays. Dashed white lines in all plots overlay the Floquet quasi-energy bands that correspond exactly to conditions in (a). Insets above the plots show the ARPES probing conditions within one pump laser cycle (with blue lines representing the x-component of $\mathbf{A}_{\mathbf{pump}}(t)$).

ARPES spectra perfectly match the theoretical model prediction, apart from a very small energy shift (<0.05 eV) between the two which arises from the employed doping procedure that shifts the chemical potential in the system. This calculation thus sets a base-line for our analysis of charge dynamics within these very same Floquet-Bloch bands that can be resolved by other types of ARPES probes.

From the Floquet theoretical point of view, the occupations of Floquet-Bloch bands are time-constant due to the underlying temporal periodicity of the pumped system. In that respect, changing the pump-probe delay in the standard conditions shown in figure 1(a) (with $f_{\text{train}}(t) = 1$) does not change the ARPES spectra as long as the two pulses temporally-overlap—the ARPES spectra in these conditions reflect the occupations of the Floquet-Bloch bands that are eigenstates of the time-averaged effective Hamiltonian. However, by utilizing an attosecond train probe pulse instead (with $f_{\text{train}}(t)$ as in equation (9)), we can track charge dynamics in those bands on a sub-laser-cycle level directly with attosecond resolution. When the temporal duration of the probe is less than one pump laser cycle, the occupation numbers of Floquet–Bloch states is no longer necessarily constant in time, because the electronic wave function in a particular moment in time is not an eigenstate of the time-averaged effective Hamiltonian. Still, since the probe samples the electron dynamics with the same temporal periodicity, we can formally use the Floquet-Bloch states as a basis set to analyze the dynamics.

Figures 2(b)–(d) shows exemplary Tr-ARPES spectra in these conditions for varying pump-probe delays. Several results are clearly apparent: (i) the Floquet–Bloch states indeed form a 'proper' basis set for the light-driven dynamics. This is clear from the ARPES spectra that follow the calculated Floquet quasi-energy bands to a very high extent for all pump-probe delays. (ii) The occupations of those Floquet-Bloch bands is different than the occupations seen in the ARPES spectra in figure 2(a), and it changes with the pump-probe delay on sub-laser-cycle timescales, which can be experimentally measured with this approach. (iii) Even though the Floquet-Bloch states are a proper basis set for the dynamics and resulting ARPES spectra, they seem to be incomplete. This becomes evident from the weaker contributions in the spectra that arise in-between the Floquet-Bloch quasi-energy bands, e.g. in the region of zero energy around K where there should not be any electronic occupations in the Floquet picture (because the system becomes gapped in the steady-state phase). These 'non-Floquet bands' appear in replica bunches that are separated by a constant energy much smaller that the pump photon energy (∼0.08 eV). In that respect, they likely hybridize the original field-free graphene bands with the Floquet bands that form in the pumped system. Thus, from this *ab-initio* calculation we can conclude that some mixed basis set is required for their analysis (which is in-line with our recent work showing that the Houston basis set is also incomplete in such conditions [51, 71]). It is also possible that intracycle interferences contribute to the non-Floquet states and enhance them. We further emphasize that these in-gap non-Floquet states do not appear in the standard conditions of Tr-ARPES (figure 2(a)), even though formally such spectra can be thought of as arising from the coherent sum of spectra at different pump-probe delays using the time-resolved attosecond train probe. This means that in standard conditions, there is a destructive interference for these electronic states over a full laser cycle that removes their contributions. From a physical perspective, the appearance of the non-Floquet bands inherently reflects a broken time-translation symmetry in the light-matter system, which might result from several different factors. The specific physical origin of 'non-Floquet-bands' will be explored in more detail in the next section 3.2.

At this stage we further analyze the temporal charge dynamics within and outside of the Floquet bands by tracking the yield of several hot-spots in the ARPES spectra while changing the pump-probe delay. Figure 3(b) presents the charge dynamics within the Floquet Bloch bands at the edges of the conduction and valence bands. The typical timescale for the dynamics is ∼1 femtosecond (whereas a single pump laser cycle in these conditions is 5.33 femtoseconds). Another observable feature is that within these dynamics the conduction and valence bands display complimentary and phase shifted dynamics, i.e. when the CB occupation increases, the valence band occupation correspondingly decreases, and vice

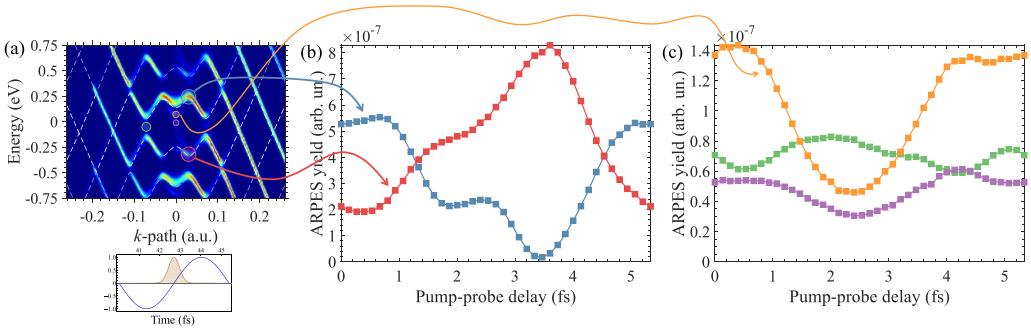

Figure 3. Sub-laser-cycle charge dynamics in Tr-ARPES spectra with a quasi-monochromatic circularly-polarized pump field (1600 nm, $I_0 = 10^{11}$ W cm^{-2}) probed parallel to k_y. (a) Tr-ARPES spectra probed by attosecond train (with f_{train}(t) as in equation (9)) for a given pump-probe delay (as in figure 2(b)). Dashed white lines overlay the Floquet quasi-energy bands that correspond exactly to conditions in figure 2(a). Inset below the spectra shows the ARPES probing conditions within one pump laser cycle (with blue lines representing the x-component of $\mathbf{A}_{\mathbf{pump}}(t)$). The highlighted colored circles in (a) represent various hot-spots in the spectra whose ARPES yield is tracked with pump-probe delay in (b) and (c) (with arrows indicating which spot is which curve), with (b) corresponding the hot-spots within Floquet-Bloch bands, and (c) to hot-spots outside of Floquet-Bloch bands.

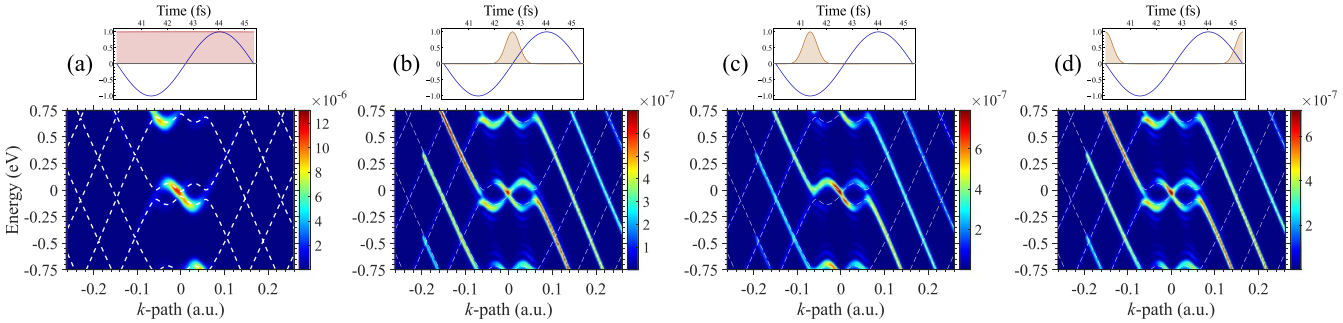

Figure 4. Tr-ARPES spectra with a quasi-monochromatic linearly-polarized pump field polarized along k$_x$ (1600 nm, $I_0 = 10^{11}$ W cm^{-2}) probed parallel to k_y. (a)–(d) Same as in figure 2, but with a linearly-polarized pump.

versa. This arises because for CPL the steady-state Floquet bands are particle-hole symmetric with opposite effective masses for electrons and holes. It can also be viewed as an analogue to rabi-oscillations, but with Floquet bands playing the major role. Figure 3(c) presents the temporal dynamics within non-Floquet bands. These also show femtosecond scale dynamics (typically ∼1 femtosecond), but with a much smaller modulation in occupation. In general, the occupations of non-Floquet bands is ∼10 times smaller than the Floquet bands throughout the dynamics.

To validate the generality of this result, we repeat our analysis in conditions where the pump laser pulse is linearly-polarized with a polarization axis parallel to k_x. In this case the Floquet quasi-energy bands take on a slightly different form with a very small gap forming at K due to a shift of the band touching points in the BZ (see [66, 72–74]). From the ARPES perspective, this gap is almost indiscernible due to resolution limitations, and there exists a finite nonzero ARPES yield at zero energy at K (see figure 4(a)). The arising light-driven charge dynamics follow similar characteristics to those in the CPL pump case, but with non-Floquet band bunches forming above and below the Floquet bands rather than in-between them. The population of the band-crossing at zero energy at K is in this case roughly independent of time (see green curve in figure 5(b)), which is a result of a mirror symmetry arising in these pump and probing conditions. Overall, similar conclusions are obtained for the linearly-polarized pumping scenario, indicating the transferability of the analysis.

3.2. *Non-Floquet-bands*

Next, we analyze the physical origin of non-Floquet bands. Let us clarify that the formation of non-Floquet states can only arise from interactions of electrons with the pump pulse. This is because the probe pulse is too weak and has too high photon energies to create such low energy scale structures in spectra. In that respect, our calculations predict that the non-Floquet bands should form in such electron dynamics regardless of the probe pulse. However, it is possible (as we will show below), that they can only be experimentally resolved by certain regimes of probe pulses, and might not be apparent if the probe pulses are too short duration, or are not pulse trains as explored here.

From a formal perspective, non-Floquet bands can only arise from time-translation symmetry breaking sources. In other words, if the dynamics were exactly time-periodic electrons would only be allowed to occupy standard Floquet-Bloch bands (which would form a complete basis-set); thus, the fact that some electrons occupy non-Floquet bands is evidence for the dynamics being not perfectly time-periodic. Within

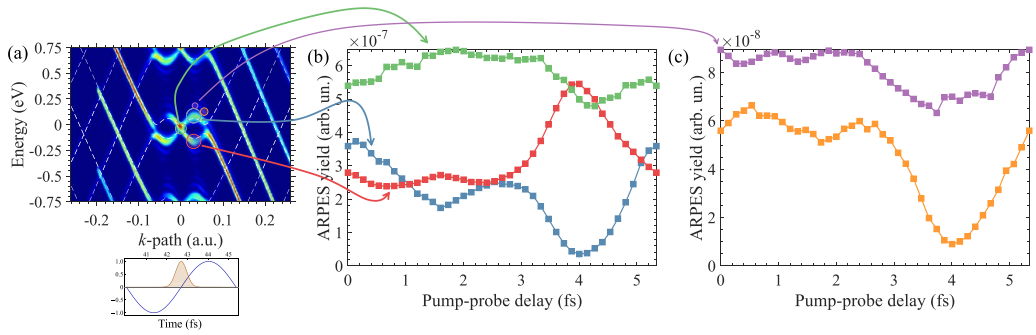

Figure 5. Sub-laser-cycle charge dynamics in Tr-ARPES spectra with a quasi-monochromatic linearly-polarized pump field polarized along k_x (1600 nm, $I_0 = 10^{11}$ W cm^{-2}) probed parallel to k_y. (a)–(c) Same as in figure 3, but with a linearly-polarized pump.

the scope of our simulation there are three possible sources for broken time-periodicity: (i) electron-electron interactions in the framework of TDDFT—due the temporal renormalization of the KS potential, time-periodicity could in principle be broken, affecting the formation of Floquet states (e.g. in a manner analogous to time-translation breaking in correlated dynamics [75–77], or in phonon-driven systems [78, 79]). Typically, such effects are weak since the KS potential renormalization is small. We have indeed found that these effects are negligible in all examined conditions for Tr-ARPES. Consequently, we rule out dynamical electron-electron interactions as a source of non-Floquet bands. (ii) Electronic excitations to the CBs—every pump laser cycle excites more electrons to higher CBs. This excited band population linearly increases with the pulse duration and builds-up over time. Thus, the population of electrons in higher bands is itself non-time-periodic, which can be prominent in the pre-thermalization Floquet phase explored here. Intuitively, it should be negligible in these conditions since the total CB occupations are minute (less than one percent of an electron per unit cell). However, it is possible that such small effects still break time-periodicity sufficiently to induce the non-Floquet bands (which are indeed an order of magnitude weaker than the main Floquet band occupations in our ARPES calculations). (iii) Pump pulse temporal laser envelope effects—even though we employ a relatively long pulse duration in the Floquet regime, the laser field is still only approximately time-periodic due to its temporal envelope. In this respect, it is possible that non-Floquet bands arise from envelope effects during the turn-on and turn-off of the Floquet phase, and represent electrons that have not managed to adiabatically enter the steady-state regime.

We now attempt to determine which of options (ii) and (iii) above dominate the formation of non-Floquet bands (or if perhaps both options contribute). For this purpose we perform a set of Tr-ARPES calculations in line with the conditions in figure 2 where the non-Floquet bands are very prominent, but where the pump laser intensity, pump temporal envelope, and the probe temporal envelope, are varied. Figure 6(a) tracks the non-Floquet band occupation as the pump laser power increases for a fixed pump-probe delay. This numerically tests sensitivity to the number of electrons excited to higher bands, because that number increases with the laser drive intensity. As shown, the non-Floquet band occupations do not consistently increase with the pump intensity. Instead, they oscillate correspondingly to the properties of the generated Floquet phase (which change with the pump power). This proves that the non-Floquet bands do not arise from symmetry breaking associated with the electronic excited population increasing over time.

Figure 6(b) shows a similar analysis of non-Floquet band occupations for a fixed delay when the pump laser envelope is tuned to induce a non-adiabatic fast turn-on of the laser pulse. The adiabaticity is controlled by changing the initial slope of the pump laser envelope (see illustration in the inset of figure 6(b)). As shown, when the envelope has a larger slope, the non-Floquet band occupation increases. This suggests it indeed arises from envelope effects of the finite pulse. We further validate this by repeating calculations and tuning the duration of the probe pulse, causing it to sample less and less pump-pulse turn-on and turn-off regions (see illustration in inset of figure 6(c)). Figure 6(c) presents the non-Floquet band occupation that is normalized to the probe pulse fluence. It shows that as the probe duration is reduced, the non-Floquet band occupation is substantially reduced, until it vanishes when the probe no longer temporally overlaps with regions around the pump pulse edges. This unequivocally shows that the non-Floquet Tr-ARPES signals arise from the envelope edges, pinpointing their physical origin to non-adiabaticity in the laser driving. We emphasize the universal importance of this result—temporal envelopes are inherent to any pulsed laser system and are often employed in experiments that generate Floquet phases.

We further note that for extremely short probe pulses we enter a regime where the Floquet phase becomes inaccessible as the probe does not sample multiple pump pulse periods. In this case the resulting ARPES spectra evolve from the Floquet picture into the Houston picture [49–51], and both Floquet and non-Floquet bands become indiscernible (see detailed data in SM).

3.3. *Polychromatic pump fields*

At this point, we extend our analysis to more complicated spatiotemporal pump waveforms that are polychromatic. Bichromatic fields were recently employed for tuning valley

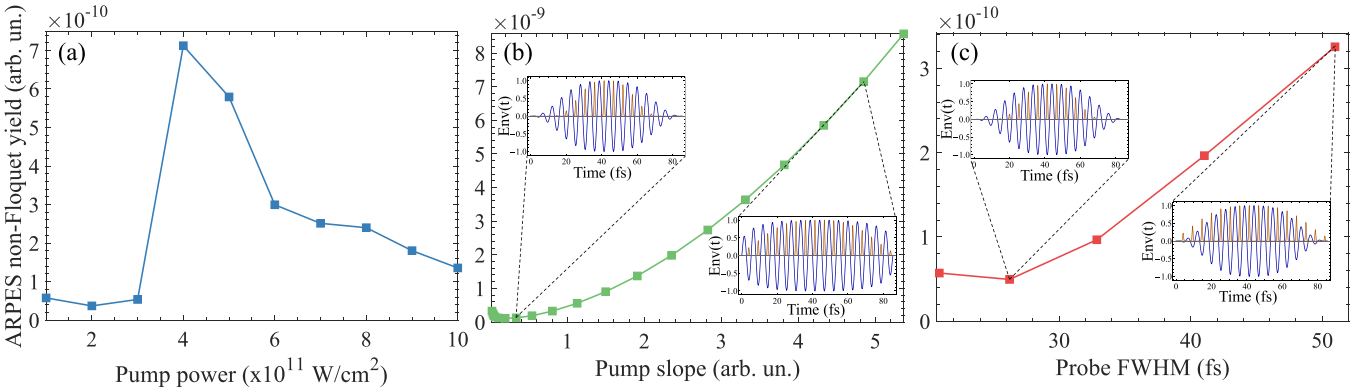

Figure 6. Non-Floquet band occupations for a fixed pump-probe delay in the same conditions as in figure 2, but for different pump and probe properties. (a) Non-Floquet band occupations for varying pump laser power. (b) Non-Floquet band occupations for varying pump pulse envelope slope. Larger slopes induce a faster pulse turn-on and turn-off, increasing non-adiabatic effects. Inset illustrates the pump pulse envelope shape changes that are simulated. (c) Non-Floquet band occupations for changing probe pulse duration (normalized to probe fluence), but while maintaining the attosecond train character of the set-up. Inset illustrates the probe pulse envelope changes that are simulated.

occupations in various systems [20, 76, 80–82], and also for dressing topological systems [7, 20, 83]. They offer a greater control of the light-matter system's symmetries, for instance breaking inversion symmetry and TRS while maintaining rotational symmetry for the CPL counter-rotating biochromatic case [68, 76]. We here use a different form of tailored pump field comprised of three carrier waves (given in equation (7)). The resulting pump field is illustrated in figure 7—due to the specific choice of relative phases between the carrier waves the electric field respects TRS over one full laser cycle. However, each individual half cycle roughly resembles CPL with opposite helicity. Our specific choice of this pump field presents an interesting test for Floquet theory in terms of sub-laser-cycle dynamics: On the one hand, the field respects TRS such that the arising Floquet quasi-energy bands should be non-gapped. On the other hand, each half-laser cycle is approximately circularly-polarized in its own right, and could form a temporally-local Floquet state with a gapped spectra (as in the quasi-monochromatic CPL case discussed above). We conceived these conditions as a numerical test for the theory, which could allow to distinguish potential sub-laser-cycle formation of Floquet physics, for which the numerical methodology derived here is ideal.

Figure 8 presents ARPES spectra dressed by the tri-chromatic pump, and probed either with a standard probe (figure 8(a)) or with an attosecond train that resolves half-pump-laser-cycles (with $f_{\text{train}}(t)$ as in equation (10), figures 8(b) and (c)). For the standard case, ARPES spectra match the Floquet quasi-energy bands extremely well (dashed white), presenting the expected behavior with no gapping of the spectrum due to TRS (see complimentary spectra probed along k_x in the supplementary material (SM)). Remarkably, the spectra probed with half-pump-laser-cycle resolution completely resembles the full-cycle case, but with a change in the Floquet occupation numbers. Certainly, spectra do not look anything like those in figure 2 which is pumped by CPL of a similar frequency to that of the CPL in each half cycle. We therefore conclude from this numerical experiment that

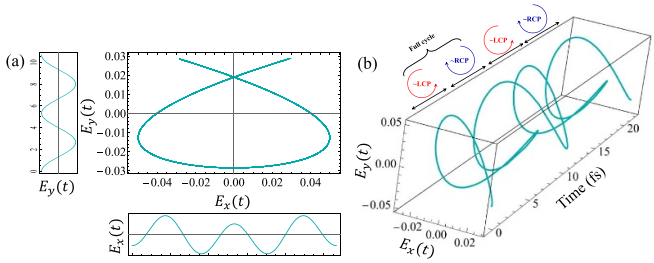

Figure 7. Illustration of tri-chromatic tailored pump laser pulse engineered by the combination of ω-2ω-3ω carrier waves with controlled polarization and relative phases (equation (7)). (a) The Lissajous curve of the pump field over one cycle, plotting the *x*–*vs*. *y*-components of the electric field and how they evolve in time. The insets on the bottom and to the left show the evolution in time of the separate field polarization components (where the *y*-component simply evolves as a 2ω sinusoidal field, and the *x*-components has more elaborate temporal evolution due to the mixture of ω and 3ω carrier waves). The Lissajous curve in (a) has a roughly circular shape, mimicking a CPL (with small deviations), but notably, flips its handedness every half cycle. (b) Electric field polarization evolving in time over two laser cycles. The field shape is seen to flip its handedness every half-cycle such that over one laser cycle TRS is upheld, but it is broken locally in time in each separate half cycle. The different regions with approximate left- or right-circular polarization (LCP, RCP) are indicated.

sub-laser-cycle Floquet states seem not to form, at least in graphene driven in these conditions (though they have been suggested in other more strongly driven materials [9]). From a physical perspective, a steady-state is simply not achieved in each separate half cycle due to the too short timescales involved, though perhaps with longer wavelength THz driving it could be reached even on separate half cycles.

We next move on to analyzing the sub-laser-cycle dynamics within the Floquet bands in the poly-chromatic pump conditions. Figures 9 and 10 present an analysis similar to that performed in the quasi-monochromatic pumping cases. In this case we see very fast charge dynamics within the

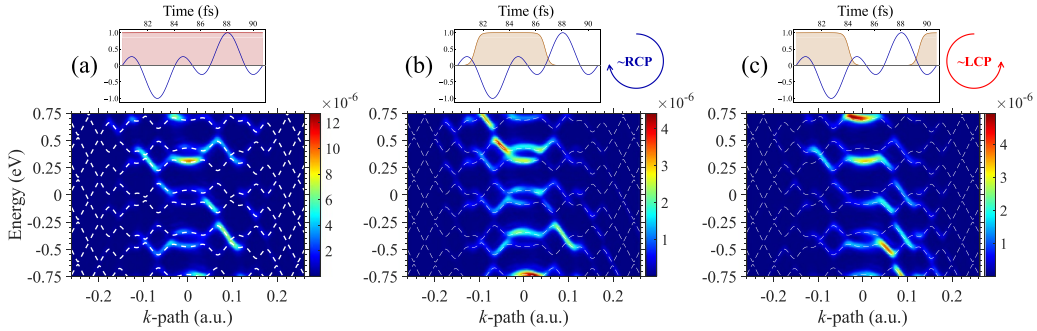

Figure 8. Tr-ARPES spectra with poly-chromatic pump field (3200 nm, $I_0 = 5{\times}10^{10}$ W cm^{-2}) probed parallel to k_y. (a) ARPES spectra in the standard conditions where sub-cycle contributions to spectra are not resolved (respecting TRS). The spectra are shifted such that the zero point indicates K. (b), (c) Tr-ARPES spectra probed by attosecond train (with f_{train}(t) as in equation (10), resolving half a pump laser cycle) for two pump-probe delays that overlap with the opposite field handedness of the half-cycles. Dashed white lines in all plots overlay the Floquet quasi-energy bands that correspond exactly to conditions in (a). Insets above the plots show the ARPES probing conditions within one pump laser cycle (with blue lines representing the x-component of $\mathbf{A}_{\mathbf{pump}}$(t)).

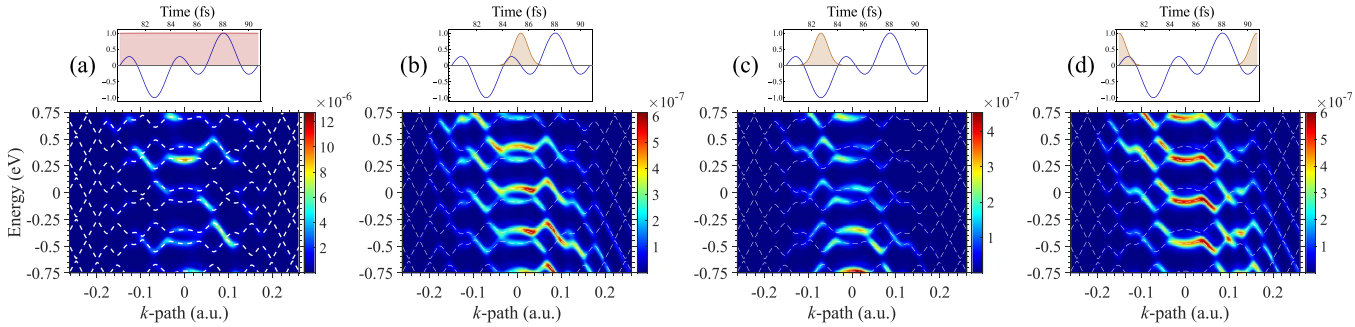

Figure 9. Tr-ARPES spectra with a polychromatic ω-2ω-3ω pump field (as in figure 7, equation (7), 3200 nm, $I_0 = 5{\times}10^{10}$ W cm^{-2}) probed parallel to k_y. (a)–(d) Same as in figure 2, but with the poly-chromatic pump.

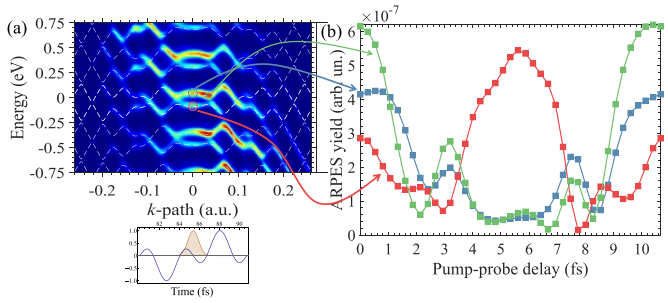

Figure 10. Sub-laser-cycle charge dynamics in Tr-ARPES spectra a polychromatic ω-2ω-3ω pump field (as in figure 6, equation (7), 3200 nm, $I_0 = 5{\times}10^{10}$ W cm^{-2}) probed parallel to k_y. (a), (b) Same as in figure 3, but with the polychromatic pump.

Floquet-Bloch states, even on timescales of ∼500 attoseconds (see figure 10(b)). This result is slightly surprising, because the fundamental carrier wave was chosen in these pumping conditions to have a similar duration of each half-pump-cycle to that of the full pump-cycle in the CPL case; hence, the electric field polarization is not evolving more rapidly in time than in standard CPL. Nonetheless, the broken symmetry field causes much faster charge motion. We further note that the charge dynamics in the valence and CBs are no longer complementary as in the CPL case (see red and blue curves in figure 10(b)), since particle-hole symmetry as broken by the broken inversion symmetry pump field.

4. Summary and outlook

To summarize, we presented an *ab-initio* study of Tr-ARPES in graphene, employing pump-probe conditions where the pump temporally overlaps with the probe. The pump pulse dresses the material electronic structure, causing it to enter into a steady-state Floquet phase of matter, while the probe pulse measures this phase and any charge dynamics driven within it. We have shown that in conditions where the probe pulse is an attosecond train with the same temporal periodicity as the pump, the delay-dependent Tr-ARPES spectra directly image the attosecond driven charge dynamics within the Floquet-Bloch states, and occupations of Floquet bands become time-dependent and immediately resolved in the ARPES data. This effect is always physically present in Floquet driven systems, but can only be imaged by using probes with a duration shorter than a pump laser cycle. We have also determined that the Floquet-Bloch states do not form a complete basis set in such a set-up, and non-Floquet bands appear in the spectra. These support similar timescale charge dynamics, and form due to

effects beyond Floquet band dressing where time-translation symmetry is broken by the finite pulse temporal envelope that induces non-adiabatic excitations. We have validated the generality and transferability of these results.

We also tested the notion of sub-laser-cycle Floquet dynamics in graphene driven by polychromatic pump pulses that overall respect TRS, but break it locally in time on half-pump-cycle timescales. We have shown that in this case, even though each half-pump-cycle behaves like circularly-polarized light, the ARPES spectra still follow the Floquet steady-state phase, and a sub-laser-cycle Floquet phase does not form. This result could help formulate a more complete approach for analyzing sub-laser-cycle attosecond dynamics in light driven systems [9, 84–87].

As a potential outlook, we believe that our numerical technique and suggested experimental set-up should motivate efforts to track charge dynamics within Floquet-Bloch bands on attosecond timescales. It should also form a basis for future work to further analyze and measure non-Floquet bands. Beyond Tr-ARPES, this work should impact neighboring fields that rely on light-driven electron dynamics such as HHG [36, 37], photogalvanic currents [35, 82, 88], and ultrafast magnetism [89, 90], where either Houston or Floquet states are used as basis sets for analyzing the dynamics. The results presented here should pave the way to a hybrid basis set for attosecond charge dynamics that combines both Houston and Floquet states, thus incorporating all physical effects on equal footing.

Data availability statement

All the data that supports the findings in this study is available in the main text and supplementary material file. Octopus code that was used for performing all of the simulations in the main texts is freely available at www.octopus-code.org. Additional data including ARPES spectrograms calculated on a finer grid of pump-probe delays is available upon reasonable request from the authors.

Acknowledgments

We acknowledge financial support from the European Research Council (ERC-2015-AdG-694097). This work was supported by the Cluster of Excellence Advanced Imaging of Matter (AIM), Grupos Consolidados (IT1249-19) and SFB925. The Flatiron Institute is a division of the Simons Foundation. O N gratefully acknowledges the generous support of a Schmidt Science Fellowship.

ORCID iDs

Ofer Neufeld https://orcid.org/0000-0002-5477-2108
Hannes Hübener https://orcid.org/0000-0003-0105-1427
Umberto De Giovannini https://orcid.org/0000-0002-4899-1304
Angel Rubio https://orcid.org/0000-0003-2060-3151

References

[1] Dóra B, Cayssol J, Simon F and Moessner R 2012 Optically engineering the topological properties of a spin hall insulator *Phys. Rev. Lett.* **108** 56602
[2] Wang Y H, Steinberg H, Jarillo-Herrero P and Gedik N 2013 Observation of floquet-bloch states on the surface of a topological insulator *Science* **342** 453–7
[3] Dehghani H, Hafezi M and Ghaemi P 2021 Light-induced topological superconductivity via Floquet interaction engineering *Phys. Rev. Res.* **3** 23039
[4] Disa A S, Nova T F and Cavalleri A 2021 Engineering crystal structures with light *Nat. Phys.* **17** 1087–92
[5] Castro A, De Giovannini U, Sato S A, Hübener H and Rubio A 2022 Floquet engineering the band structure of materials with optimal control theory *Phys. Rev. Res.* **4** 33213
[6] Lu M, Reid G H, Fritsch A R, Piñeiro A M and Spielman I B 2022 Floquet engineering topological dirac bands *Phys. Rev. Lett.* **129** 40402
[7] Trevisan T V, Arribi P V, Heinonen O, Slager R-J and Orth P P 2022 Bicircular light floquet engineering of magnetic symmetry and topology and its application to the dirac semimetal Cd_3As_2 *Phys. Rev. Lett.* **128** 66602
[8] Bhattacharya U, Chaudhary S, Grass T, Johnson A S, Wall S and Lewenstein M 2022 Fermionic Chern insulator from twisted light with linear polarization *Phys. Rev.* B **105** L081406
[9] Uzan-Narovlansky A *et al* 2022 Observation of light-driven band structure via multiband high-harmonic spectroscopy *Nat. Photon.* **16** 428–32
[10] Bloch J, Cavalleri A, Galitski V, Hafezi M and Rubio A 2022 Strongly correlated electron–photon systems *Nature* **606** 41–48
[11] Esin I, Rudner M S and Lindner N H 2023 Floquet metal-to-insulator phase transitions in semiconductor nanowires *Sci. Adv.* **6** eaay4922
[12] Topp G E, Jotzu G, McIver J W, Xian L, Rubio A and Sentef M A 2019 Topological Floquet engineering of twisted bilayer graphene *Phys. Rev. Res.* **1** 1–12
[13] Hübener H, Sentef M A, De Giovannini U, Kemper A F and Rubio A 2017 Creating stable Floquet-Weyl semimetals by laser-driving of 3D Dirac materials *Nat. Commun.* **8** 13940
[14] Nag T, Slager R-J, Higuchi T and Oka T 2019 Dynamical synchronization transition in interacting electron systems *Phys. Rev.* B **100** 134301
[15] Oka T and Kitamura S 2019 Floquet engineering of quantum materials *Annu. Rev. Condens. Matter Phys.* **10** 387–408
[16] Nathan F, Abanin D, Berg E, Lindner N H and Rudner M S 2019 Anomalous Floquet insulators *Phys. Rev.* B **99** 195133
[17] Frisk Kockum A, Miranowicz A, De Liberato S, Savasta S and Nori F 2019 Ultrastrong coupling between light and matter *Nat. Rev. Phys.* **1** 19–40
[18] Rudner M S and Lindner N H 2020 Band structure engineering and non-equilibrium dynamics in Floquet topological insulators *Nat. Rev. Phys.* **2** 229–44
[19] Rodriguez-Vega M, Vogl M and Fiete G A 2020 Floquet engineering of twisted double bilayer graphene *Phys. Rev. Res.* **2** 33494
[20] Jiménez-Galán Á, Silva R E F, Smirnova O and Ivanov M 2020 Lightwave control of topological properties in 2D materials for sub-cycle and non-resonant valley manipulation *Nat. Photon.* **14** 728–32
[21] Shan J-Y, Ye M, Chu H, Lee S, Park J-G, Balents L and Hsieh D 2021 Giant modulation of optical nonlinearity by Floquet engineering *Nature* **600** 235–9
[22] Holthaus M 2016 Floquet engineering with quasienergy bands of periodically driven optical lattices *J. Phys. B: At. Mol. Opt. Phys.* **49** 13001

[23] Lindner N H, Refael G and Galitski V 2010 Floquet topological insulator in semiconductor quantum wells *Nat. Phys.* **7** 490–5

[24] Kitagawa T, Oka T, Brataas A, Fu L and Demler E 2011 Transport properties of nonequilibrium systems under the application of light: photoinduced quantum Hall insulators without Landau levels *Phys. Rev.* B **84** 235108

[25] Rechtsman M C, Zeuner J M, Plotnik Y, Lumer Y, Podolsky D, Dreisow F, Nolte S, Segev M and Szameit A 2013 Photonic Floquet topological insulators *Nature* **496** 196–200

[26] Rudner M S, Lindner N H, Berg E and Levin M 2014 Anomalous edge states and the bulk-edge correspondence for periodically driven two-dimensional systems *Phys. Rev.* X **3** 1–15

[27] Kundu A, Fertig H A and Seradjeh B 2014 Effective theory of floquet topological transitions *Phys. Rev. Lett.* **113** 236803

[28] Usaj G, Perez-Piskunow P M, Foa Torres L E F and Balseiro C A 2014 Irradiated graphene as a tunable Floquet topological insulator *Phys. Rev.* B **90** 115423

[29] Grushin A G, Gómez-León Á and Neupert T 2014 Floquet fractional Chern insulators *Phys. Rev. Lett.* **112** 156801

[30] Titum P, Lindner N H, Rechtsman M C and Refael G 2015 Disorder-induced floquet topological insulators *Phys. Rev. Lett.* **114** 056801

[31] Bradlyn B, Elcoro L, Cano J, Vergniory M G, Wang Z, Felser C, Aroyo M I and Bernevig B A 2017 Topological quantum chemistry *Nature* **547** 298–305

[32] Vergniory M G, Elcoro L, Felser C, Regnault N, Bernevig B A and Wang Z 2019 A complete catalogue of high-quality topological materials *Nature* **566** 480–5

[33] McIver J W, Schulte B, Stein F-U, Matsuyama T, Jotzu G, Meier G and Cavalleri A 2020 Light-induced anomalous Hall effect in graphene *Nat. Phys.* **16** 38–41

[34] Sato S A *et al* 2019 Microscopic theory for the light-induced anomalous Hall effect in graphene *Phys. Rev.* B **99** 214302

[35] Higuchi T, Heide C, Ullmann K, Weber H B and Hommelhoff P 2017 Light-field-driven currents in graphene *Nature* **550** 224–8

[36] Yue L and Gaarde M B 2022 Introduction to theory of high-harmonic generation in solids: tutorial *J. Opt. Soc. Am.* B **39** 535–55

[37] Ghimire S and Reis D A 2019 High-harmonic generation from solids *Nat. Phys.* **15** 10–16

[38] Aeschlimann S *et al* 2021 Survival of Floquet–bloch states in the presence of scattering *Nano Lett.* **21** 5028–35

[39] Zhou S *et al* 2023 Pseudospin-selective Floquet band engineering in black phosphorus *Nature* **614** 75–80

[40] Mahmood F, Chan C-K, Alpichshev Z, Gardner D, Lee Y, Lee P A and Gedik N 2016 Selective scattering between Floquet–Bloch and Volkov states in a topological insulator *Nat. Phys.* **12** 306–10

[41] Soifer H *et al* 2019 Band-resolved imaging of photocurrent in a topological insulator *Phys. Rev. Lett.* **122** 167401

[42] Reimann J *et al* 2018 Subcycle observation of lightwave-driven Dirac currents in a topological surface band *Nature* **562** 396–400

[43] Ossiander M *et al* 2018 Absolute timing of the photoelectric effect *Nature* **561** 374–7

[44] Heinrich S, Saule T, Högner M, Cui Y, Yakovlev V S, Pupeza I and Kleineberg U 2021 Attosecond intra-valence band dynamics and resonant-photoemission delays in W(110) *Nat. Commun.* **12** 3404

[45] Tao Z, Chen C, Szilvási T, Keller M, Mavrikakis M, Kapteyn H and Murnane M 2016 Direct time-domain observation of attosecond final-state lifetimes in photoemission from solids *Science* **353** 62–67

[46] Lloyd-Hughes J *et al* 2021 The 2021 ultrafast spectroscopic probes of condensed matter roadmap *J. Phys.: Condens. Matter* **33** 353001

[47] Lucchini M *et al* 2022 Controlling Floquet states on ultrashort time scales *Nat. Commun.* **13** 7103

[48] Ito S *et al* 2023 Build-up and dephasing of Floquet–Bloch bands on subcycle timescales *Nature* **616** 696–701

[49] Houston W V 1940 Acceleration of electrons in a crystal lattice *Phys. Rev.* **57** 184–6

[50] Krieger J B and Iafrate G J 1986 Time evolution of Bloch electrons in a homogeneous electric field *Phys. Rev.* B **33** 5494–500

[51] Neufeld O, Mao W, Hübener H, Tancogne-Dejean N, Sato S A, De Giovannini U and Rubio A 2022 Time- and angle-resolved photoelectron spectroscopy of strong-field light-dressed solids: prevalence of the adiabatic band picture *Phys. Rev. Res.* **4** 033101

[52] Bukov M and Polkovnikov A 2014 Stroboscopic versus nonstroboscopic dynamics in the Floquet realization of the harper-hofstadter hamiltonian *Phys. Rev.* A **90** 43613

[53] Goldman N and Dalibard J 2014 Periodically driven quantum systems: effective Hamiltonians and engineered gauge fields *Phys. Rev.* X **4** 31027

[54] Anisimovas E, Žlabys G, Anderson B M, Juzeliūnas G and Eckardt A 2015 Role of real-space micromotion for bosonic and fermionic Floquet fractional Chern insulators *Phys. Rev.* B **91** 245135

[55] Bukov M, D'Alessio L and Polkovnikov A 2015 Universal high-frequency behavior of periodically driven systems: from dynamical stabilization to Floquet engineering *Adv. Phys.* **64** 139–226

[56] Desbuquois R, Messer M, Görg F, Sandholzer K, Jotzu G and Esslinger T 2017 Controlling the Floquet state population and observing micromotion in a periodically driven two-body quantum system *Phys. Rev.* A **96** 53602

[57] Paul P M, Toma E S, Breger P, Mullot G, Augé F, Balcou P, Muller H G and Agostini P 2001 Observation of a train of attosecond pulses from high harmonic generation *Science* **292** 1689–92

[58] Agostini P and DiMauro L F 2004 The physics of attosecond light pulses *Rep. Prog. Phys.* **67** 813

[59] Marques M A L, Ullrich C A, Nogueira F, Rubio A, Burke K and Gross E K U 2003 *Time-Dependent Density Functional Theory, Time-Dependent Density Functional Theory* (Springer)

[60] Marques M A L, Castro A, Bertsch G F and Rubio A 2003 octopus: a first-principles tool for excited electron–ion dynamics *Comput. Phys. Commun.* **151** 60–78

[61] Castro A, Appel H, Oliveira M, Rozzi C A, Andrade X, Lorenzen F, Marques M A L, Gross E K U and Rubio A 2006 octopus: a tool for the application of time-dependent density functional theory *Phys. Status Solidi* **243** 2465–88

[62] Andrade X *et al* 2015 Real-space grids and the Octopus code as tools for the development of new simulation approaches for electronic systems *Phys. Chem. Chem. Phys.* **17** 31371–96

[63] Tancogne-Dejean N *et al* 2020 Octopus, a computational framework for exploring light-driven phenomena and quantum dynamics in extended and finite systems *J. Chem. Phys.* **152** 124119

[64] Hartwigsen C, Goedecker S and Hutter J 1998 Relativistic separable dual-space Gaussian pseudopotentials from H to Rn *Phys. Rev.* B **58** 3641–62

[65] De Giovannini U, Larsen A H and Rubio A 2015 Modeling electron dynamics coupled to continuum states in finite volumes with absorbing boundaries *Eur. Phys. J.* B **88** 56

[66] Neufeld O, Hübener H, Jotzu G, Giovannini De U and Rubio A 2023 Band nonlinearity-enabled manipulation of Dirac nodes, Weyl cones, and valleytronics with intense linearly polarized light *Nano Lett.* **23** 7568–75

[67] Neufeld O and Cohen O 2019 Background-free measurement of ring currents by symmetry-breaking high-harmonic spectroscopy *Phys. Rev. Lett.* **123** 103202
[68] Neufeld O, Podolsky D and Cohen O 2019 Floquet group theory and its application to selection rules in harmonic generation *Nat. Commun.* **10** 405
[69] Scrinzi A 2012 T-SURFF: fully differential two-electron photo-emission spectra *New J. Phys.* **14** 085008
[70] De Giovannini U, Hübener H and Rubio A 2017 A first-principles time-dependent density functional theory framework for spin and time-resolved angular-resolved photoelectron spectroscopy in periodic systems *J. Chem. Theory. Comput.* **13** 265–73
[71] Galler A, Rubio A and Neufeld O 2023 Mapping light-dressed Floquet bands by highly nonlinear optical excitations and valley polarization *J. Phys. Chem. Lett.* **14** 11298–304
[72] Koghee S, Lim L-K, Goerbig M O and Smith C M 2012 Merging and alignment of Dirac points in a shaken honeycomb optical lattice *Phys. Rev.* A **85** 23637
[73] Jotzu G, Messer M, Desbuquois R, Lebrat M, Uehlinger T, Greif D and Esslinger T 2014 Experimental realization of the topological Haldane model with ultracold fermions *Nature* **515** 237–40
[74] Delplace P, Gómez-León Á and Platero G 2013 Merging of Dirac points and Floquet topological transitions in ac-driven graphene *Phys. Rev.* B **88** 245422
[75] Tancogne-Dejean N, Sentef M A and Rubio A 2018 Ultrafast modification of Hubbard U in a strongly correlated material: ab initio high-harmonic generation in NiO *Phys. Rev. Lett.* **121** 097402
[76] Neufeld O, Tancogne-Dejean N, De Giovannini U, Hübener H and Rubio A 2021 Light-driven extremely nonlinear bulk photogalvanic currents *Phys. Rev. Lett.* **127** 126601
[77] Baykusheva D R *et al* 2022 Ultrafast renormalization of the on-site coulomb repulsion in a cuprate superconductor *Phys. Rev.* X **12** 11013
[78] Rana N and Dixit G 2022 Probing phonon-driven symmetry alterations in graphene via high-order-harmonic spectroscopy *Phys. Rev.* A **106** 53116
[79] Neufeld O, Zhang J, De Giovannini U, Hübener H and Rubio A 2022 Probing phonon dynamics with multidimensional high harmonic carrier-envelope-phase spectroscopy *Proc. Natl Acad. Sci.* **119** e2204219119
[80] Mrudul M S, Jiménez-Galán Á, Ivanov M and Dixit G 2021 Light-induced valleytronics in pristine graphene *Optica* **8** 422–7
[81] Sharma S, Elliott P and Shallcross S 2023 THz induced giant spin and valley currents *Sci. Adv.* **9** eadf3673
[82] Ikeda Y, Kitamura S and Morimoto T 2023 Photocurrent induced by a bicircular light drive in centrosymmetric systems *Phys. Rev. Lett.* **131** 96301
[83] Wang Y, Walter A-S, Jotzu G and Viebahn K 2023 Topological Floquet engineering using two frequencies in two dimensions *Phys. Rev.* A **107** 043309
[84] Uzan A J *et al* 2020 Attosecond spectral singularities in solid-state high-harmonic generation *Nat. Photon.* **14** 183–7
[85] Lakhotia H, Kim H Y, Zhan M, Hu S, Meng S and Goulielmakis E 2020 Laser picoscopy of valence electrons in solids *Nature* **583** 55–59
[86] Freudenstein J *et al* 2022 Attosecond clocking of correlations between Bloch electrons *Nature* **610** 290–5
[87] Langer F *et al* 2016 Lightwave-driven quasiparticle collisions on a subcycle timescale *Nature* **533** 225–9
[88] Langer F *et al* 2020 Few-cycle lightwave-driven currents in a semiconductor at high repetition rate *Optica* **7** 276–9
[89] Siegrist F *et al* 2019 Light-wave dynamic control of magnetism *Nature* **571** 240–4
[90] Neufeld O, Tancogne-Dejean N, De Giovannini U, Hübener H and Rubio A 2023 Attosecond magnetization dynamics in non-magnetic materials driven by intense femtosecond lasers *npj Comput. Mater.* **9** 39